Diffraction and conversion of elastic waves at a corrugated interface

Anne Paul* and Michel Campillo*

ABSTRACT

Numerical modeling is used to investigate the effect of small-scale irregularities of a reflecting boundary on elastic wave reflections. The scattered wave field is computed by using a discretized form of boundary integral equations and a plane-wave decomposition of seismic wave fields. For various values of incidence angle of the P wave, we compute the distribution of diffracted energy for both P waves and S waves as a function of reflection angle. We show that corrugations with mean wavelength of the order of, or smaller than, the seismic wavelength have little effect on the reflected P wave. However, the pattern of P-to-S conversion is very different from that with a plane boundary. Scattered S waves appear at postcritical angles for any angle of incidence of the P wave. The amplitude of these nongeometrical shear waves decreases rapidly with decreasing amplitude of the corrugations, or when the mean wavelength of the corrugations becomes larger than the dominant seismic wavelength. The local geometry of the irregularities has a negligible effect on the scattered S waves. By analogy with perturbation theory, we propose interpreting the postcritically scattered S waves as the contribution to the shear wave field of converted inhomogeneous P waves diffracted along the boundary.

INTRODUCTION

The effects of lateral heterogeneities within the Earth have been recognized at all scales and types of seismic data. Many attempts have been made to simulate realistically wave propagation which accounts for the diffraction phenomena produced by these irregularities. Most existing methods belong to one of the following two classes: In the deterministic approach, forward modeling (e.g., ray theory) is applied to structures with known geometries, i.e., to large-scale heterogeneities. In the statistical approach, the lithosphere is viewed as an unbounded medium whose physical parameters vary weakly and in a random fashion (e.g., Chernov, 1960; Wu and Aki, 1985); perturbation theory is used to investigate elastic wave scattering in such media.

However, the case of an elastic boundary affected by corrugations whose size is of the order of a wavelength has not been subjected to extended studies. None of the two above-cited approaches is applicable to this particular problem. The first method requires a deterministic definition of the geometry of inhomogeneities, while the statistical approach is restricted to models with a homogeneous and unbounded reference medium. We combine the two approaches by applying forward modeling to a medium whose elastic parameters vary randomly. This modeling makes it possible to deal with scattering by complex structures such as an elastic interface bearing irregularities of small and randomly varying size. Interfaces of this type are of interest, since they could cause many observed anomalies, such as the generation of S waves from explosive sources and the abnormal reflectivity of some subsurface boundaries. Scattering by a rough interface could be a source of coda waves; corrugations of the Mohorovicic discontinuity could explain the long wavetrains of reflections from the lower crust frequently observed in both wide-angle and vertical seismic recordings of the continental crust.

Previous work includes Asano's (1966) application of the Rayleigh method to study the reflection of a quasi-vertically incident plane P wave on an irregular interface with periodic corrugations. Hill and Levander (1984) used finite-difference simulations of SH-wave propagation in a medium with irregular buried interfaces to show that energy trapped within a low-velocity layer bounded by corrugated interfaces could contribute largely to the coda of the signal.

In this paper, our aim is to evaluate, for an incident P wave, the reflected P and SV waves from a boundary with small-scale corrugations between two elastic media. We vary parameters such as amplitude, wavelength, geometry of the irregularities, and the impedance contrast at the boundary. Computations are performed following the approach initiated by Bouchon (1985) and Campillo and Bouchon (1985) for the simulation of SH-wave propagation in a medium with an ir-

regular boundary. This treatment is extended to the *P-SV* case.

THE GENERALIZED REFLECTION COEFFICIENTS

In the following sections, the term "reflection coefficient" stands for an amplitude ratio for Lamb potentials. For a plane wave incident with horizontal wavenumber k_i upon a perfectly smooth boundary, the reflection coefficient $R(k_i)$ gives the amplitude of the potential associated with the reflected plane wave with the same horizontal wavenumber k_i; $R(k_i)$ is a general notation for $R_{PP}(k_i)$ or $R_{PS}(k_i)$ depending on the type of reflected wave.

In the presence of an irregular boundary, incident energy is diffusely scattered into directions corresponding to horizontal wavenumbers k_r with $k_r \neq k_i$. Following Hill and Levander (1984), we define the generalized reflection coefficient $r(k_i, k_r)$ as the potential associated with the k_r component of the scattered wave field for a plane wave of wavenumber k_i incident from above. Descartes' law thus gives for a perfectly smooth boundary

$$r(k_i, k_r) = \delta(k_r - k_i)R(k_i),$$

where $\delta(k_r - k_i)$ is the Dirac delta function. The diffracting effects of the corrugations will be described in the following sections by (a) the difference between the amplitude of the specularly reflected wave from the corrugated surface $r(k_i, k_i)$, and that from the smooth surface $R(k_i)$, (b) amplitudes of the irregularly reflected waves $r(k_i, k_r)$ with $k_i \neq k_r$.

METHOD OF COMPUTATION

Solution of the general problem of a diffracting interface

The basic principles and some applications of the method for *SH* waves incident upon a diffracting boundary have been presented by Campillo and Bouchon (1985) and Campillo (1987). Their approach relies on the simultaneous use of a discretized form of boundary integral equations and plane-wave decomposition of seismic wave fields.

The geometry of the problem is depicted in Figure 1. An irregular interface C separates two infinite elastic media (1) and (2). In order to reduce the problem to 2-D, the interface is assumed to be uniform in the y direction. The compressional and shear-wave velocities are denoted by α_i and β_i, respec-
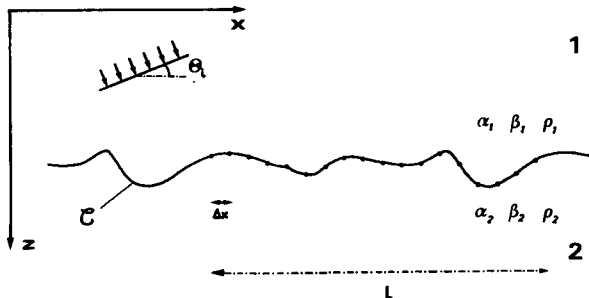

FIG. 1. Geometry of the problem. Boundary C is periodic with repetition length L. Discretization interval is Δx.

tively, and the densities by ρ_i. A plane wave propagating in medium (1) impinges upon the boundary at incidence angle θ_i.

Following the principle of boundary methods (Brebbia, 1978), diffracted wave fields are represented in both media by the radiation of a distribution of body forces $F^{(i)}(x, z)$ applied along the interface. The strength of each force is computed so as to match boundary conditions. Continuity of displacements and stresses along C implies

$$u^{(1)}(x, z) = u^{(2)}(x, z),$$

$$w^{(1)}(x, z) = w^{(2)}(x, z),$$

$$n_x \tau_{xx}^{(1)} + n_z \tau_{xz}^{(1)} = n_x \tau_{xx}^{(2)} + n_z \tau_{xz}^{(2)}, \tag{1}$$

and

$$n_x \tau_{xz}^{(1)} + n_z \tau_{zz}^{(1)} = n_x \tau_{xz}^{(2)} + n_z \tau_{zz}^{(2)}$$

for every point $M(x, z)$ on C. $u^{(i)}(x, z)$ and $w^{(i)}(x, z)$ are the horizontal and vertical components of the displacement field in medium (i). $\tau_{ij}^{(i)}$ is component (i, j) of the stress tensor for medium (i) and (n_x, n_z) are the coordinates of the vector normal to C at M. Displacement fields are computed using the following decomposition:

$$u^{(1)}(x, z) = u_C^{(1)}(x, z) + u_s^{(1)}(x, z),$$

$$w^{(1)}(x, z) = w_C^{(1)}(x, z) + w_s^{(1)}(x, z),$$

$$u^{(2)}(x, z) = u_C^{(2)}(x, z), \tag{2}$$

and

$$w^{(2)}(x, z) = w_C^{(2)}(x, z),$$

where $(u_s^{(1)}, w_s^{(1)})$ denotes the displacement associated with the incident wave field and $(u_C^{(i)}, w_C^{(i)})$, the displacements associated with the diffracted field in medium (i).

Let $G_{uv}^{(i)}(x, z; x', z')$ be the set of Green's functions of medium (i). $u_C^{(i)}(x, z)$ and $w_C^{(i)}(x, z)$ can be expressed as functions of the horizontal and vertical components $F_H^{(i)}$ and $F_V^{(i)}$ of body forces $F^{(i)}(x, z)$:

$$u_C^{(i)}(x, z) = \int_C \left[F_H^{(i)}(x', z')G_{xx}^{(i)}(x, z; x', z') \right.$$

$$\left. + F_V^{(i)}(x', z')G_{zx}^{(i)}(x, z; x', z') \right] d\ell$$

$$w_C^{(i)}(x, z) = \int_C \left[F_H^{(i)}(x', z')G_{xz}^{(i)}(x, z; x', z') \right. \tag{3}$$

$$\left. + F_V^{(i)}(x', z')G_{zz}^{(i)}(x, z; x', z') \right] d\ell.$$

Note that a 2-D problem is being solved using the infinite-space Green's function for a line source.

The numerical solution of equations (3) requires a discretization of the boundary C. To this end, body forces are applied at equal spacing Δx along C (Figure 1). The optimal value of Δx is a function of the steepest dip along the interface and the frequency of the seismic wave. According to earlier studies (Campillo, 1987), three points per shortest wavelength (i.e., shear wavelength in the slowest medium) are sufficient. Tests with up to five points per wavelength confirm this observation. Integrals are thus replaced by discrete summations in equations (3) to give

$$u_C^{(i)}(x, z) = \sum_{m=-\infty}^{+\infty} \left[F_H^{(i)}(x_m, z_m) G_{xx}^{(i)}(x, z; x_m, z_m) \right.$$
$$\left. + F_V^{(i)}(x_m, z_m) G_{zx}^{(i)}(x, z; x_m, z_m) \right]$$

and $\qquad\qquad\qquad\qquad\qquad\qquad\qquad\qquad$ (4)

$$w_C^{(i)}(x, z) = \sum_{m=-\infty}^{+\infty} \left[F_H^{(i)}(x_m, z_m) G_{xz}^{(i)}(x, z; x_m, z_m) \right.$$
$$\left. + F_V^{(i)}(x_m, z_m) G_{zz}^{(i)}(x, z; x_m, z_m) \right].$$

Green's functions are computed using a decomposition of wave fields into plane waves. We assume the source medium configuration to be periodic along the x axis with repetition length L. The radiation of each body force is computed in the frequency domain using the discrete wavenumber method (Bouchon and Aki, 1977). If one period L of the boundary C is represented by an array of $2M + 1$ points, we have from equation (4)

$$u_C^{(i)}(x, z) = \frac{-i}{2L\omega^2\rho_i} \left\{ \sum_{m=-M}^{M} F_H^{(i)}(x_m, z_m) \right.$$

$$\times \sum_{p=-\infty}^{+\infty} \left[\frac{k_p^2}{v_p^{(i)}} \exp\left(-iv_p^{(i)}|z-z_m|\right) + \gamma_p^{(i)} \exp\left(-i\gamma_p^{(i)}|z-z_m|\right) \right]$$

$$\times \exp\left[-ik_p(x - x_m)\right] + \sum_{m=-M}^{M} F_V^{(i)}(x_m, z_m) \operatorname{sgn}(z - z_m)$$

$$\times \sum_{p=-\infty}^{+\infty} k_p \left[\exp\left(-iv_p^{(i)}|z - z_m|\right) - \exp\left(-i\gamma_p^{(i)}|z - z_m|\right) \right]$$

$$\left. \times \exp\left[-ik_p(x - x_m)\right] \right\}, \qquad\qquad (5)$$

with

$$k_p = \frac{2\pi}{L} p,$$

$$v_p^{(i)} = \left(\frac{\omega^2}{\alpha_i^2} - k_p^2 \right)^{1/2}, \qquad \operatorname{Im}(v_p^{(i)}) \leq 0$$

$$\gamma_p^{(i)} = \left(\frac{\omega^2}{\beta_i^2} - k_p^2 \right)^{1/2}, \qquad \operatorname{Im}(\gamma_p^{(i)}) \leq 0,$$

where ω is the angular frequency. A similar expression can be derived for the vertical component of the displacement $w_C^{(i)}(x, z)$.

As we write the boundary conditions (1) at any discrete point along C, we will necessarily encounter the well-known problem of the stress field discontinuity at the point of application of a force. Bouchon (1985) and Campillo and Bouchon (1985) have shown that those singularities can be avoided in practice by using truncated Fourier series in place of the actual Green's function in equation (5). This can be physically interpreted as the substitution for line sources (whose Green's functions are infinite series with respect to k_p) by spatially extended sources (whose Green's functions are truncated Fourier series). Bouchon (1987) has shown the accuracy of the method in the elastic case by means of comparisons to other solutions for the diffraction by cracks.

Combining equation (5) (with truncated summations over k_p) and a similar expression for $w_C^{(i)}(x, z)$ with boundary conditions (1) yields a system of four equations per point within one period L of the boundary C,

$$A_C^{(1)}(x_r, z_r) - A_C^{(2)}(x_r, z_r) = A_s^{(1)}(x_r, z_r), \quad 1 \leq r \leq 2M + 1,$$
$$\qquad\qquad\qquad\qquad\qquad\qquad\qquad (6)$$

where A is a general notation for the components of displacement and stress fields. We now have a system of $8M + 4$ linear equations for the $8M + 4$ unknown values of the strengths $F_H^{(i)}(x_m, z_m)$, $F_V^{(i)}(x_m, z_m)$ of the fictitious sources along C. This system is solved directly.

The effect of medium periodicity can be attenuated in the frequency domain by adding a small negative imaginary part to the frequency and can be completely removed from the time-domain solution (Bouchon and Aki, 1977).

As shown by equation (5), this approach relies on the global consideration of the whole set of sources along the interface in the expression of the boundary conditions at one particular point. Nonlocal effects such as refracted or multiply reflected waves are thus accounted for with this method, ensuring the completeness of the solution.

Evaluation of generalized reflection coefficients

We shall use Lamb potentials to calculate reflection coefficients. Noting that $u = \partial\phi/\partial x - \partial\psi/\partial z$ and $w = \partial\Phi/\partial z + \partial\Psi/\partial x$, we obtain the compressional and rotational potentials associated with the wave field diffracted in medium (i)

$$\Phi_C^{(i)}(x, z) = \frac{1}{2L\omega^2\rho_i} \sum_{m=-M}^{+M} \left(F_{H,m}^{(i)} \sum_{p=-M}^{+M} \frac{k_p}{v_p^{(i)}} \right.$$

$$\times \exp\left\{ -i\left[v_p^{(i)}|z - z_m| + k_p(x - x_m) \right] \right\}$$

$$+ F_{V,m}^{(i)} \operatorname{sgn}(z - z_m)$$

$$\left. \times \sum_{p=-M}^{+M} \exp\left\{ -i\left[v_p^{(i)}|z - z_m| + k_p(x - x_m) \right] \right\} \right)$$

$$\Psi_C^{(i)}(x, z) = \frac{1}{2L\omega^2\rho_i} \sum_{m=-M}^{+M} \left(-F_{H,m}^{(i)} \operatorname{sgn}(z - z_m) \right.$$

$$\times \sum_{p=-M}^{+M} \exp\left\{ -i\left[\gamma_p^{(i)}|z - z_m| + k_p(x - x_m) \right] \right\}$$

$$\left. + F_{V,m}^{(i)} \sum_{p=-M}^{+M} \frac{k_p}{\gamma_p^{(i)}} \exp\left\{ -i\left[\gamma_p^{(i)}|z - z_m| + k_p(x - x_m) \right] \right\} \right),$$
$$\qquad\qquad\qquad\qquad\qquad\qquad\qquad (7)$$

where $F_{H,m}^{(i)}$ and $F_{V,m}^{(i)}$ are simplified notations for $F_H^{(i)}(x_m, z_m)$ and $F_V^{(i)}(x_m, z_m)$.

It appears from these equations that the diffracted wave fields are not uniquely decomposable into plane waves at any point $M(x, z)$ within the medium. However, if the observation point is chosen at a sufficient distance from the interface, $\operatorname{sgn}(z - z_m)$ is constant for every point $S(x_m, z_m)$ on the boundary. The decomposition into plane waves can then be performed. For an observation point in medium (1), we may

change the summation order in equation (7) to obtain

$$\Phi_C^{(1)}(x, z) = \frac{1}{2L\omega^2\rho_1} \sum_{p=-M}^{+M} \left\{ \sum_{m=-M}^{+M} \left(F_{H,m}^{(1)} \frac{k_p}{v_p^{(1)}} - F_{V,m}^{(1)} \right) \right.$$
$$\times \exp\left[-i(v_p^{(1)}z_m - k_p x_m)\right]\Big\}$$
$$\times \exp\left[-i(-v_p^{(1)}z + k_p x)\right]$$

and

$$\Psi_C^{(1)}(x, z) = \frac{1}{2L\omega^2\rho_1} \sum_{p=-M}^{+M} \left\{ \sum_{m=-M}^{+M} \left(F_{H,m}^{(1)} + F_{V,m}^{(1)} \frac{k_p}{\gamma_p^{(1)}} \right) \right.$$
$$\times \exp\left[-i(\gamma_p^{(1)}z_m - k_p x_m)\right]\Big\}$$
$$\times \exp\left[-i(-\gamma_p^{(1)}z + k_p x)\right]. \tag{8}$$

These relations show that the diffracted wave field can be decomposed into a discrete sum of plane P waves and S waves. The amplitudes of their associated potentials are given by

$$\phi^{(1)}(k_p) = \frac{1}{2L\omega^2\rho_1} \sum_{m=-M}^{+M} \left(F_{H,m}^{(1)} \frac{k_p}{v_p^{(1)}} - F_{V,m}^{(1)} \right)$$
$$\times \exp\left[-i(v_p^{(1)}z_m - k_p x_m)\right]$$

and

$$\psi^{(1)}(k_p) = \frac{1}{2L\omega^2\rho_1} \sum_{m=-M}^{+M} \left(F_{H,m}^{(1)} + F_{V,m}^{(1)} \frac{k_p}{\gamma_p^{(1)}} \right)$$
$$\times \exp\left[-i(\gamma_p^{(1)}z_m - k_p x_m)\right], \tag{9}$$

where $k_p = (2\pi/L)p$ is the discrete horizontal wavenumber.

The generalized reflection coefficients $r(k_i, k_r)$ are defined as the amplitude ratios of the potentials associated with the diffracted field to the one corresponding to the incident field. Their computation is done in two steps:

(a) calculation of the body forces distributions $F_{H,m}^{(1)}$, $F_{V,m}^{(1)}$ for unit-amplitude plane-wave incidence with horizontal wavenumber k_i and

(b) calculation of the reflection coefficients

$$r_P(k_i, k_r) = \phi^{(1)}(k_r)$$

and

$$r_S(k_i, k_r) = \psi^{(1)}(k_r).$$

Computations are performed for all positive values of the discrete wavenumbers k_i and k_r associated with plane waves propagating in the positive x direction.

RESULTS: GENERALIZED REFLECTION COEFFICIENTS

Most of the computations are carried out for a corrugated interface which is constant in the y direction and where x_z variation is described by

$$z = \xi(x) = z_0 + \frac{h_i}{2} \sin\left(\frac{2\pi}{\ell_i} x\right) \quad \text{for} \sum_{j=1}^{i-1} \ell_j \leq x < \sum_{j=1}^{i} \ell_j, \tag{10}$$

with

$$h_i = h(1 + \varepsilon_i)$$

and

$$\ell_i = \ell(1 + \varepsilon_i),$$

where z_0 is the depth of the smooth boundary, h is the peak-to-peak mean amplitude of the corrugations, ℓ is their mean wavelength, and ε_i is a random number between -0.5 and $+0.5$.

The interface is constructed from equation (10) by dividing a period L of the source-medium configuration into N sinusoidal corrugations. The mean wavelength $\ell = L/N$. A series of N values is chosen for ε_i, each one being associated with a particular period of the corrugations. These values are introduced in the expressions for h_i and ℓ_i and $\xi(x)$ is calculated from equation (10). We obtain an interface made up of a series of sinusoidal cycles whose wavelengths ℓ_i and amplitudes h_i vary around the mean values h and ℓ. An example of this geometry is depicted in Figure 2a. This choice allows a closed-form expression for a realistic corrugated boundary. Equation (10) is a compromise between perfectly periodic corrugations ($\varepsilon_i = 0$) and random lateral variation of the boundary. Moreover, the introduction of ε_i attenuates the destructive interference induced by a periodic reflector (Bragg's X-ray diffraction law).

Our aim was to study the influence on the $P_M P$ phase (reflection from the Mohorovicic discontinuity) of hypothetical corrugations on this boundary. Since these reflections have frequencies around 20 Hz, all the computations have been
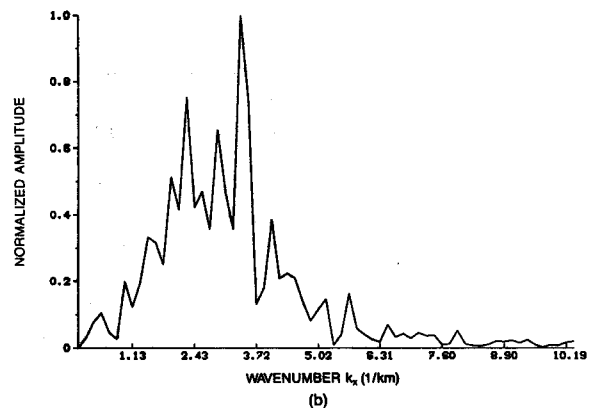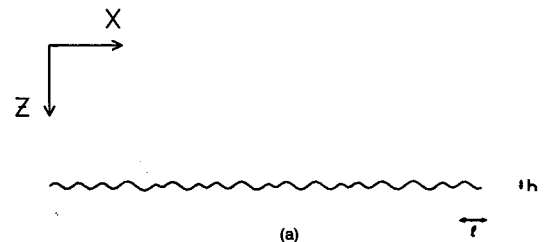

FIG. 2. Reference model. (a) Geometry of the corrugated interface for $\ell = 0.89 \ WL$ and $h = 0.25 \ WL$. (b) Normalized amplitude spectrum of the rough boundary. Peak amplitude corresponds to the mean wavelength ℓ of the corrugations.

carried out at this frequency. Effects of corrugations with sizes between a few tens and a hundred meters have been studied. Nevertheless, these results may be generalized to any other frequency and any other size of corrugations. The ratio of the size of the irregularities to WL, the wavelength of the incident wave, is the only relevant parameter.

A specific interface with fixed geometrical parameters ($\ell = 0.89\ WL$, $h = 0.25\ WL$) and fixed impedance contrast representative of the Moho discontinuity ($\alpha_1 = 6.7$ km/s, $\beta_1 = 3.9$ km/s, $\rho_1 = 3.$; $\alpha_2 = 8.2$ km/s, $\beta_2 = 4.7$ km/s, $\rho_2 = 3.3$) is used as a reference model. We compare computations of generalized reflection coefficients for different amplitudes, wavelengths, and geometries of corrugations and different velocity models with those of our first model.

Reference model

The interface geometry and its amplitude spectrum are plotted in Figure 2. It is clear from Figure 2b that we may expect incident energy to be scattered in all directions, since a wide range of horizontal wavenumber k_x is covered.

Figure 3 shows generalized reflection coefficients $r_{PP}(k_i,\ k_r)$ and $r_{PS}(k_i,\ k_r)$ plotted with respect to incidence angle θ_i of the incident P wave [$\theta_i = \sin^{-1}(\alpha_1 k_i/\omega)$] and reflection angle θ_r of diffracted P waves or S waves [$\theta_r = \sin^{-1}(ck_r/\omega)$, $c = \alpha_1$ or β_1]. A comparison with the corresponding values of reflection coefficients for a perfectly smooth boundary is presented. $R_{PP}(\theta_i)$ and $R_{PS}(\theta_i)$ are computed from expressions given by Aki and Richards (1980).
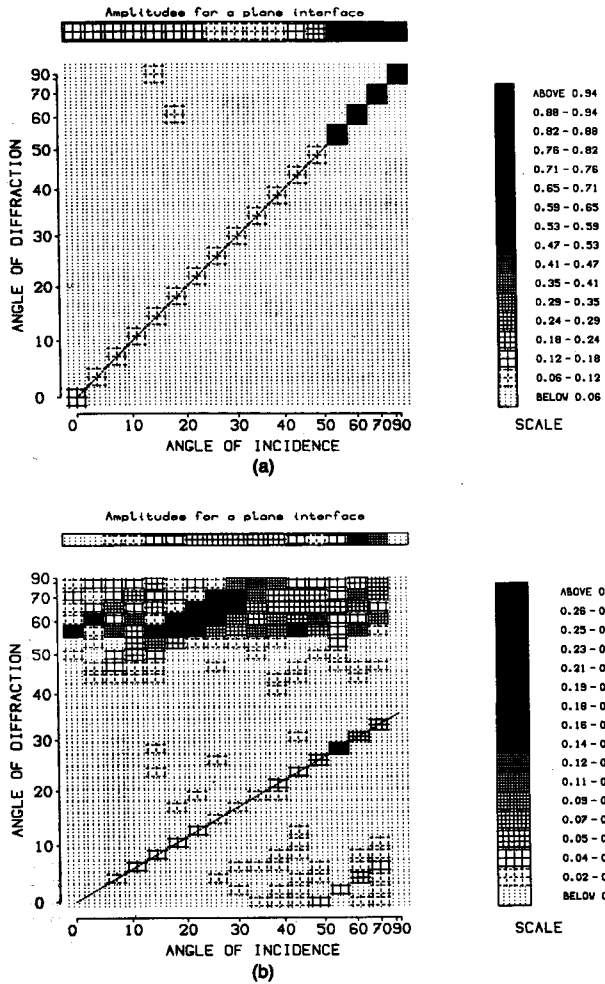

FIG. 3. Amplitudes of the generalized reflection coefficients (a) $r_{PP}(\theta_i,\ \theta_r)$ and (b) $r_{PS}(\theta_i,\ \theta_r)$ for the reference model. They are plotted as functions of the incidence angle of the incident plane P wave θ_i and of the reflection angle of diffracted P wave or S wave θ_r. For comparison with a smooth interface, values of theoretical reflection coefficients $R_{PP}(\theta_i)$ or $R_{PS}(\theta_i)$ are plotted on top of both figures. For a plane boundary, those values would occur along the oblique line indicated on the plots. P-wave reflection is mostly specular, but anomalous converted S waves are apparent at angles greater than 55 degrees.
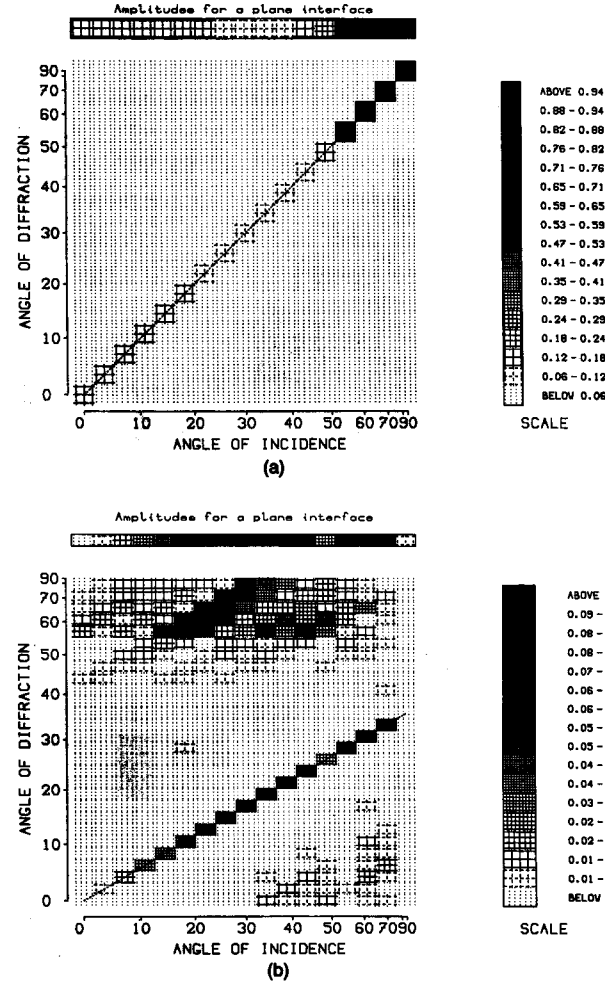

FIG. 4. Same as Figure 3. Generalized reflection coefficients are plotted for the case of low-amplitude corrugations ($h = 0.10\ WL$). Comparison with Figure 3 shows a clear decrease in the amplitude of scattered S waves.

It is clear from Figure 3 that the diffracted S wave is much more affected by the presence of corrugations than the diffracted P wave. r_{PP} has significant values only along the diagonal line of the plot, showing that most of the energy is reflected specularly. Since the presence of irregularities causes a weak loss of specular energy, $r_{PP}(\theta_i, \theta_i)$ is always lower than $R_{PP}(\theta_i)$. Very little incident energy is scattered in irregular directions above 55 degrees, mainly for small incidence angles.

However, the highest values of the r_{PS} coefficient occur for angles greater than the maximum angle for specular P-to-S reflection on the smooth interface, i.e., $\theta_m = 36$ degrees. Most energy is scattered at angles greater than 55 degrees irrespective of the P-wave incidence angle. The highest values of r_{PS}

concentrate along a line parallel to the one corresponding to Descartes' law. This results from the quasi-periodicity of the corrugations. The random variations of width and height in equation (10) attenuate Bragg's effect but do not eliminate it. The difference in the amplitudes of specular reflections $R_{PS} - r_{PS}$ varies randomly with θ_i. For some values of θ_i (e.g., between 20 and 40 degrees), this difference is negative, whereas it is positive for $\theta_i = 54$ degrees. These results agree with, and even generalize to, a wider range of incidence angles, the results obtained by Asano (1966).

Effect of the amplitude of corrugations

The results from using a lower value of the mean amplitude of irregularities, $h = 0.1 \ WL$, are shown in Figure 4. Effects of
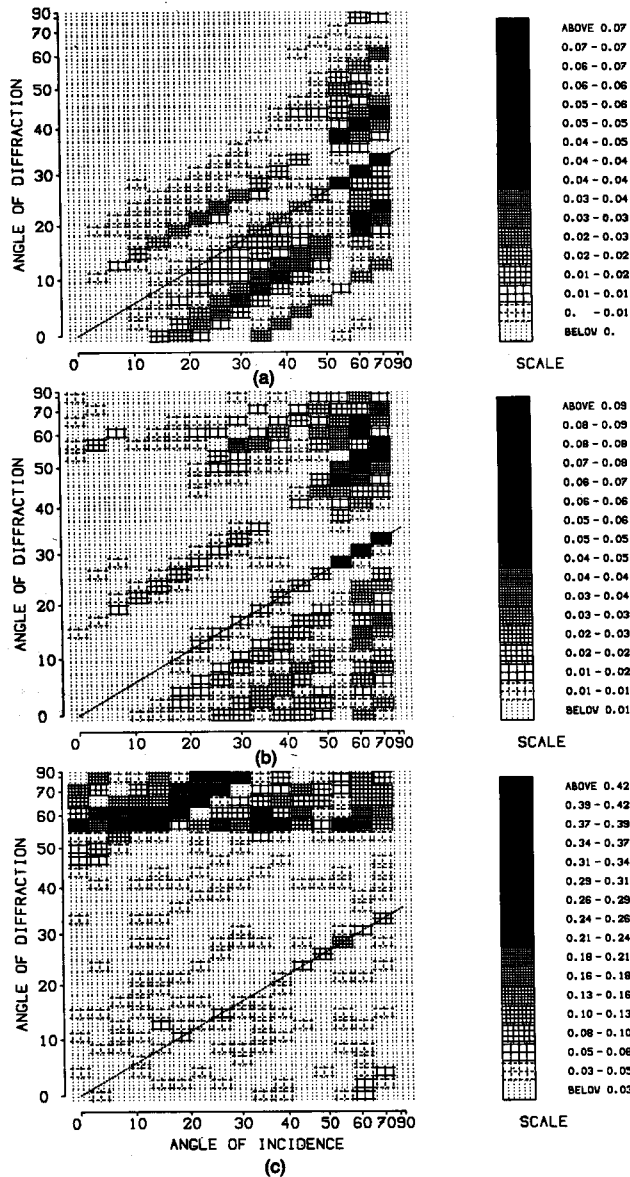

FIG. 5. Effect of the corrugation wavelength on the reflection coefficient r_{PS}. (a) $\ell = 4 \ WL$; scattered energy is spread out around the specular reflection. (b) $\ell = 2.3 \ WL$; scattering in angles greater than 55 degrees becomes apparent. (c) $\ell = 0.8 \ WL$; most of the shear energy is concentrated above 55 degrees.
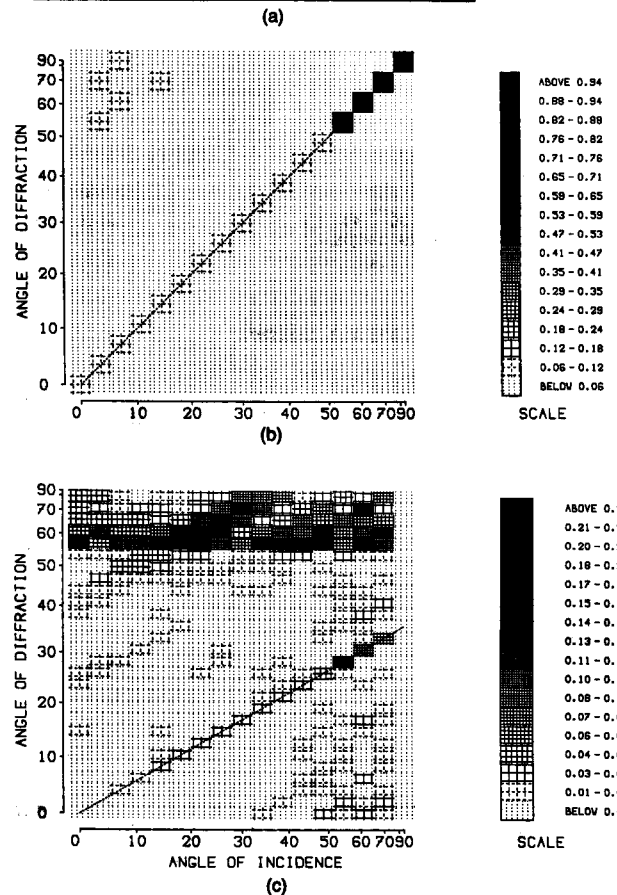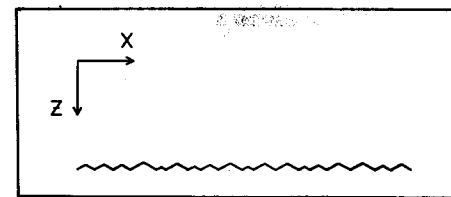
FIG. 6. (a) New geometry of the boundary, with triangular shaped corrugations. Corresponding values of generalized reflection coefficients (b) r_{PP} and (c) r_{PS}. Comparison with Figure 3 shows only little variation in the diffraction pattern as a result of modification of the geometry.

Amplitudes for a plane interface

ANGLE OF DIFFRACTION

ANGLE OF INCIDENCE

(a)

	ABOVE 0.94
	0.88 - 0.94
	0.82 - 0.88
	0.76 - 0.82
	0.71 - 0.76
	0.65 - 0.71
	0.59 - 0.65
	0.53 - 0.59
	0.47 - 0.53
	0.41 - 0.47
	0.35 - 0.41
	0.29 - 0.35
	0.24 - 0.29
	0.18 - 0.24
	0.12 - 0.18
	0.06 - 0.12
	BELOW 0.06

SCALE

Amplitudes for a plane interface

ANGLE OF DIFFRACTION

ANGLE OF INCIDENCE

(b)

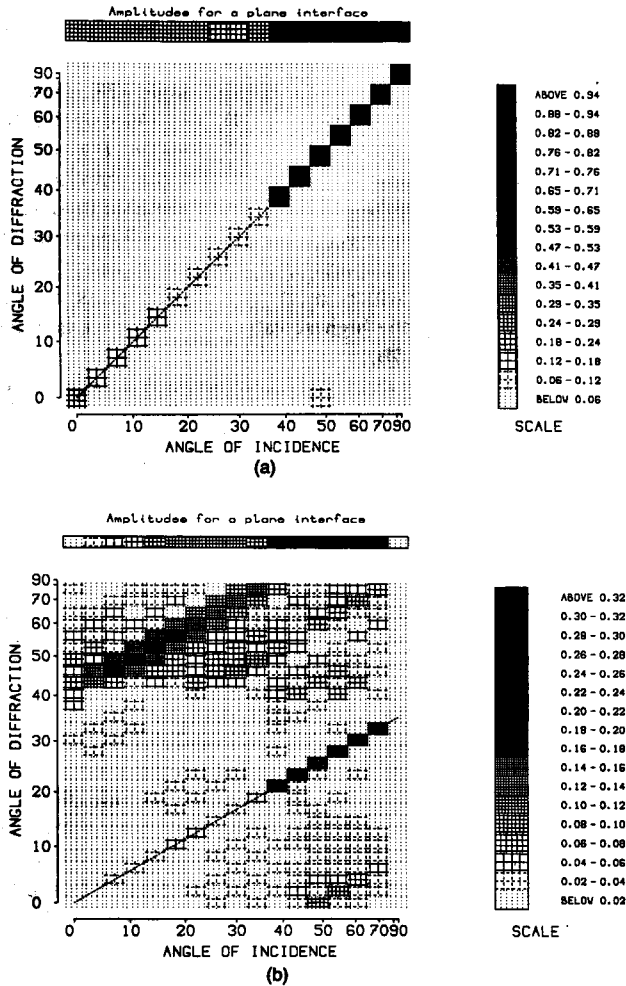|	
	ABOVE 0.32
	0.30 - 0.32
	0.28 - 0.30
	0.26 - 0.28
	0.24 - 0.26
	0.22 - 0.24
	0.20 - 0.22
	0.18 - 0.20
	0.16 - 0.18
	0.14 - 0.16
	0.12 - 0.14
	0.10 - 0.12
	0.08 - 0.10
	0.06 - 0.08
	0.04 - 0.06
	0.02 - 0.04
	BELOW 0.02

SCALE

FIG. 7. Reflection coefficients for an interface with higher impedance contrast. A wider range of diffraction angles is now affected by the anomalously scattered S waves.
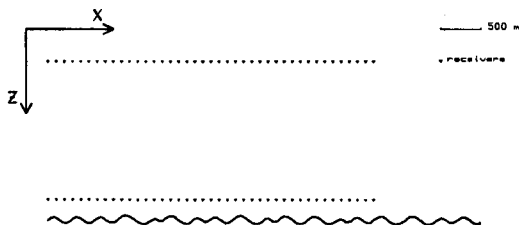

FIG. 8. Geometry of the boundary and locations of receivers used in computations of synthetic seismograms. Receivers with a 100 m spacing are situated 250 and 2000 m above the interface. Values for the boundary are $h = 85$m and $\ell = 298$ m.

corrugations have nearly disappeared on the r_{PP} plot; $r_{PP}(\theta_i, \theta_i)$ and $R_{PP}(\theta_i)$ exhibit little difference. P-wave reflection is mostly specular. The S wave field scattered at high angles is still visible, but amplitudes of the corresponding reflection coefficients are less than one-half of those in Figure 3. Their highest values are now of the order of magnitude of $r_{PS}(\theta_i, \theta_i')$, where θ_i' represents the S-wave specular reflection angle for an incident P wave with angle θ_i. The difference between $R_{PS}(\theta_i)$ and $r_{PS}(\theta_i, \theta_i')$ remains constant and low as θ_i varies. For this low value of h, the reflection pattern is very similar to the one for a smooth boundary.

Effect of the corrugation wavelength

For the same amplitude h and three values of ℓ ranging from 4 WL to 0.8 WL, the amplitudes of reflection coefficients r_{PS} are plotted in Figure 5. For $\ell = 4$ WL (Figure 5a), diffracted energy is spread out in the vicinity of the specular angle of reflection; specular reflection coefficients are significantly lower than for a smooth interface. With decreasing ℓ (Figure 5b), the anomalous pattern of P-to-S conversion for θ^n above 55 degrees occurs, while energy scattered below the specular angle of reflection weakens. Finally, Figure 5c shows a spectacular concentration of converted P- to S-wave energy for angles above 55 degrees.

Influence of the geometry of corrugations

The geometry of the boundary was modified in two ways. We first changed the series of random numbers ε_i, keeping the same values for h and ℓ. The amplitudes of reflection coefficients changed little, and the overall characteristics of the diffracted wave fields were preserved.

The geometry of corrugations was modified by replacing the sine function in $\xi(x)$ by a triangular shaped function. The new geometry and values of reflection coefficients are given in Figure 6. We are led to the same conclusion as before: for small-scale corrugations with respect to incident wavelength, the local geometry of the boundary has a negligible effect on the scattering of P waves and S waves. The simulations of Hill and Levander (1984) show a similar scattering of both transmitted and reflected waves into postcritical directions. Since they used a third geometry of corrugations (crenellations), their results confirm our conclusion.

Effect of the impedance contrast

For a stronger contrast, we investigated whether anomalous P-to-S conversion still occurred. The model considered is as follows: $\alpha_1 = 2.5$ km/s, $\beta_1 = 1.45$ km/s, $\rho_1 = 2.1$; $\alpha_2 = 4.$ km/s, $\beta_2 = 2.3$ km/s, $\rho_2 = 2.4$. The ratios of the mean amplitude and the mean wavelength of corrugations to the wavelength of the incident P wave ($\ell = 0.89$ WL, $h = 0.25$ WL) are held constant. Results are depicted in Figure 7.

Irregularly reflected S waves are still apparent but a wider range of diffraction angles is now affected beginning at 38 degrees. This points out the major part played by the critical angle of P-to-P (or S-to-S) reflection on the smooth interface. The change in velocity contrast results precisely in shifting this

Horizontal   Vertical

(a)   z = 250m

Horizontal   Vertical

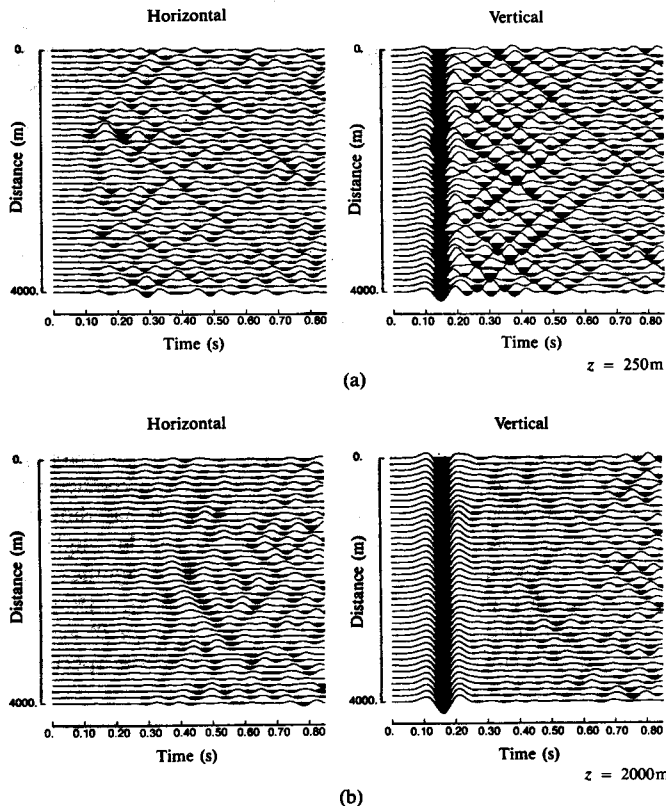(b)   z = 2000m

FIG. 9. Horizontal and vertical components of the displacement field associated with diffraction of a vertically incident plane P wave for the geometry of Figure 8. The two displacement fields correspond to two values of z, the distance between the receivers and the interface. The time window is a 0.85 s wide moving window positioned with respect to the arrival time of the reflected P wave.

Horizontal   Vertical

z = 250m

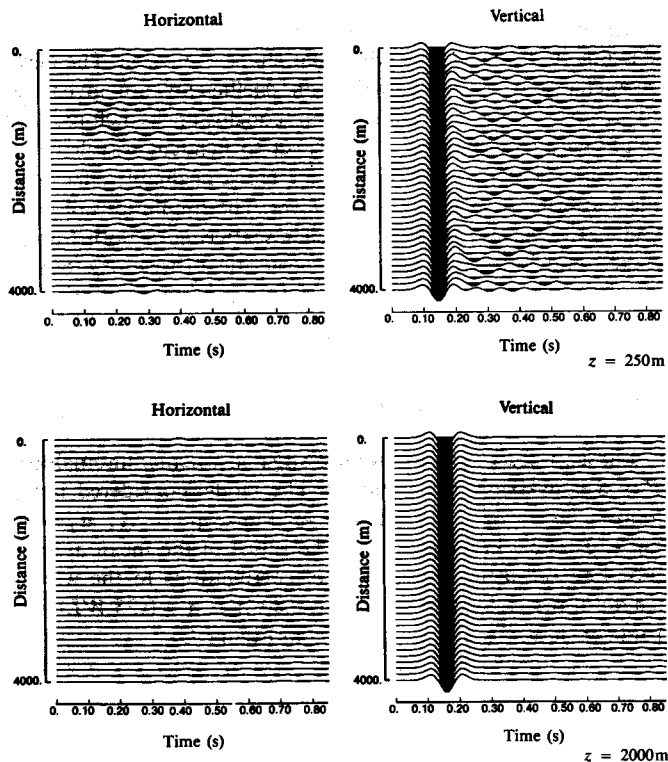Horizontal   Vertical

z = 2000m

Fig. 10. Same as Figure 9. Corrugations amplitude is $h = 35$ m.

angle from 55 to 38 degrees. It is worth noting that this result agrees with the postcritical nature of scattered SH waves in Hill and Levander's simulations.

For both the PP as well as the PS reflection, it appears that the decrease in reflection coefficients $R(\theta_i) - r(\theta_i, \theta_i')$ is more important for a larger velocity contrast. One may note however that when θ_i reaches the critical angle (38 degrees), $r_{PS}(\theta_i, \theta_i')$ reaches a higher value than $R_{PS}(\theta_i)$. Once again, this generalizes Asano's results for a vertically incident P wave.

Asano's computations also showed that the amplitude of the so-called first irregular wave, or first harmonic in Bragg's law, was enhanced by a larger velocity contrast. This phenomenon is clear from a comparison of Figures 3b and 7b. This first irregular wave, which is shown on the plots by the oblique line carrying the highest values of $r_{PS}(\theta_i, \theta_r)$, is much more visible in Figure 7b.

Besides these high values, the ratio between amplitudes of scattered S waves and specularly reflected waves is, on the average, lower for a larger velocity contrast. We conclude that postcritical scattering of S waves becomes weaker, in comparison to the specular reflection, for an increasing impedance contrast.

INTERPRETATION

Our interpretation of this anomalous P-to-S conversion is based on synthetic seismic sections. Calculations are first carried out for a vertically incident plane P wave on the reference interface ($\ell = 298$ m and $h = 85$ m). The velocity contrast corresponds to the Mohorovicic discontinuity. Seismic displacement fields are simulated along two profiles located 250 and 2000 m above the corrugated boundary as shown in Figure 8. Transfer functions are computed in the frequency domain between 0 and 20 Hz. The source function used is a Ricker wavelet with peak frequency $f_0 = 8$ Hz. The resulting synthetic seismograms are plotted in Figure 9. We repeated the computations for low-amplitude corrugations ($h = 35$ m). Corresponding results are presented in Figure 10.

Figures 9 and 10 show the prominent arrival of the specularly reflected P wave. In Figure 9 it is followed by scattered energy with large amplitude. The distinctive feature of this diffracted wave field is its high coherency from trace to trace resulting in a characteristic crisscross pattern. We may note that Figure 8 in Hill and Levander (1984) shows a very similar pattern of waveguide modes in a low-velocity layer with irregular boundaries. Numerous plane waves seem to propagate forward and backward symmetrically at an angle of 55 to 60 degrees from the vertical. As seen in Figure 3, a significant part of the energy of a vertically incident P wave is converted into S waves with a reflection angle of about 56 degrees. We conclude that the plane waves observed in Figure 9 correspond to the postcritically converted S waves. This conclusion is confirmed by Figure 10, where diffracted waves are indeed weaker for low-amplitude corrugations.

In Figure 9a, where the receivers are close to the interface, diffracted waves interfere with the specularly reflected P wave. This results in apparent time shifts of the P-wave arrival. Figure 9b shows that the separation of arrival times between reflected P waves and diffracted S waves increases when the receivers are farther from the interface. Their arrival times are
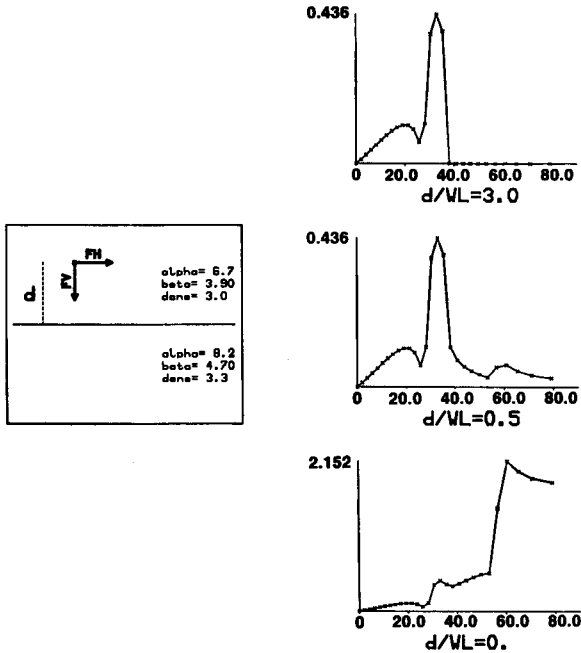
the P wavelength, the energy is radiated at angles greater than θ_m. Figure 11b shows a prominent peak just above the critical angle $\theta_c = 55$ degrees. For d equal to zero, this effect is accentuated. As seen in Figure 11c, the highest amplitudes of the P-to-S converted wave are emitted at angles greater than 60 degrees, i.e., in postcritical directions. $d = 0$ corresponds precisely to the case of fictitious sources applied over the boundary to compute the diffracted field. Figure 11c reflects the influence of the evanescent P waves converted to postcritically emitted S waves at the interface.

Some of these characteristics resemble those of the S^* wave as predicted by Hron and Mikhailenko (1981). S^* is generated by an explosive source buried less than one wavelength from the free surface or any other interface. It is interpreted by the above-cited authors as the result of the interaction between the reflector and inhomogeneous P waves emitted by the source.

S^* and our diffracted S have a number of common characteristics. Both are shear waves converted from compressional waves. They propagate with angles restricted to values greater than $\theta_m = \sin^{-1}(\beta/\alpha)$. Both S^* and diffracted S are nongeometrical waves. They are the contribution to the converted S wave field of inhomogeneous P waves radiated by the source or by diffracting points on the rough boundary.

This interpretation is made clearer by applying the pertubation method to this problem. This method is based on the decomposition of the wave field into primary waves (unperturbed term) and scattered waves (perturbed term). Primary waves satisfy the wave equation for the unperturbed medium (homogeneous medium without diffracting bodies). Scattered waves are the solution of the same equation with a body force. The strength of this force is computed from the values of the perturbations affecting the density and Lamé constants of the medium $\partial\rho(x, z)$, $\partial\mu(x, z)$, $\partial\lambda(x, z)$. The perturbation method thus accounts for diffracting bodies with equivalent body forces. In the case of a diffracting interface, we consider the superposition of two semiinfinite media in contact through a plane boundary as the unperturbed medium. We have shown that the diffracted wave field may be interpreted as the sum of radiations of secondary point sources located along the interface. These fictitious sources play the same part as the equivalent body forces of the perturbation method. The main difference is the existence of a plane boundary in the unperturbed medium. As a consequence, the Green's function for a point source on a plane boundary, and not the Green's function for an unbounded medium, must be considered in the representation of the diffracted field. In Figure 11c, we showed that this particular Green's function (for a source on the boundary) has significant energy beyond the critical angle. The sources on the rough boundary thus generate evanescent compressional waves that are converted to far-field shear waves analogous to the S^*.

FIG. 11. Amplitudes of the rotational potential associated with S waves converted at the interface from P waves radiated by a point source. Amplitudes are plotted as functions of the azimuth measured from the vertical. The three curves correspond to three different values of the ratio between the source-interface distance d and the wavelength WL.

clearly related to that of the specularly reflected S wave. A detailed observation of horizontal components in Figure 9 shows that these seemingly plane waves are in fact branches of diffraction hyperbolas whose apices are tangential to the arrival time of the specular S wave.

This result is reminiscent of the exploding reflector concept basis for migration, such as Kirchhoff summation (Schneider, 1978). Each point of a reflector is considered to be a secondary source, and the input data are correlated with the point-source response for a homogeneous medium, i.e., a hyperbolic operator. However, our results show that the diffracting boundary does not behave as an assemblage of isotropic point sources. If this were the case, we would expect energy to be homogeneously distributed along diffraction hyperbolas. However, S waves exhibit a quite different behavior, with the interface radiating much more energy at angles greater than the critical angle.

To interpret this phenomenon, we computed the amplitudes of the reflection potentials associated with wave fields radiated by a point source. The source consists of two orthogonal equal forces F_H and F_V located in a semiinfinite medium at distance d from a plane interface. d is first given a large value with respect to the P wavelength and diminished progressively. The amplitude of the rotational potential associated with the P- to S-converted wave at the interface is plotted in Figure 11 as a function of the reflection angle. For $d = 3\ WL$, no energy is emitted at angles greater than $\theta_m = 36$ degrees. This value corresponds to the reflection angle of the reflected S wave for a horizontally incident P wave [$\theta_m = \sin^{-1}(\beta/\alpha)$]. Any reflection energy at angles greater than θ_m must result from evanescent waves radiated by the source. If d is less than

CONCLUSIONS

Using a discretized form of boundary integral equations, we simulated the scattering of incident P waves by an irregular boundary with small-scale corrugations with respect to the incident wavelength. Generalized reflection coefficients were

computed for different roughness geometries and velocity contrasts. Reflected P waves are weakly affected by the presence of irregularities. However, the rate of P-to-S conversion is modified in a nonnegligible way. For certain dimensions of corrugations, the reflection coefficient for converted shear waves may even reach the value of the reflection coefficient for specularly reflected P waves. Such converted S waves are emitted at angles greater than the critical. Their amplitudes decrease rapidly with decreasing amplitude of corrugations. Like S^*, these scattered S waves are the contribution of inhomogeneous P waves to the converted shear wave field.

The magnitude of this conversion phenomenon is a clear indication of the importance of considering full-wave elastic scattering in the simulations of seismic diffraction. There is no doubt that irregular elastic interfaces with small-scale corrugations exist within the Earth. This scattered S wave field may help to provide answers to a number of important questions. Computations of synthetic seismic sections have shown that these waves could contribute significantly to the coda of seismograms. Moreover, such postcritical S waves may explain the abnormally high amplitudes of Lg waves radiated from explosions. A corrugated interface in the vicinity of the source contributes much more efficiently in the postcritically converted shear wave field than does a smooth boundary. The critical S waves are then trapped within the crust to create high-amplitude Lg phases.

Within the framework of exploration seismology, the ability of rough boundaries to induce efficient P-to-S conversion explains the generation of shear waves from explosions (e.g., Fertig, 1984). This phenomenon may also contribute significantly to the degradation of the signal-to-noise ratio resulting from excitation of waveguide modes in the weathered zone.

Finally these results show that hectometric corrugations of the Mohorovicic discontinuity cannot explain the presence of laminated reflections visible on many deep seismic profiles of the continental crust (Bois et al., 1987). Such heterogeneities have indeed a negligible effect on the PP reflected wave field.

ACKNOWLEDGMENTS

REFERENCES

Aki, K., and Richards, P. G., 1980, Quantitative seismology, theory and methods: W. H. Freeman and Co.

Asano, S., 1966, Reflection and refraction of elastic waves at a corrugated interface: Bull. Seis. Soc. Am., 56, 201–221.

Bois, C., Cazes, M., Hirn, A., Mascle, A., Matte, P., Montadert, L., and Pinet, B., 1987, Contribution of deep seismic profiling to the knowledge of the lower crust in France and neighbouring areas: Tectonophys., 145, 253–275.

Bouchon, M., 1985, A simple, complete numerical solution to the problem of diffraction of SH waves by an irregular surface: J. Acoust. Soc. Am., 77, 1–5.

—— 1987, Diffraction of elastic waves by cracks or cavities using the discrete wavenumber method: J. Acoust. Soc. Am., 81, 1671–1676.

Bouchon, M., and Aki, K., 1977, Discrete wavenumber representation of seismic source wavefield: Bull. Seis. Soc. Am., 67, 259–277.

Brebbia, C. A., 1978, The boundary element method for engineers: Pentech Press.

Campillo, M., 1987, Modeling of SH-wave propagation in an irregularly layered medium; application to seismic profiles near a dome: Geophys. Prosp., 35, 236–249.

Campillo, M., and Bouchon, M., 1985, Synthetic SH seismograms in a laterally varying medium by the discrete wavenumber method: Geophys. J. Roy. Astr. Soc., 83, 307–317.

Chernov, L. A., 1960, Wave propagation in a random medium: McGraw-Hill Book Co.

Fertig, J., 1984, Shear waves by an explosive point-source; the earth surface as a generator of converted P-S waves: Geophys. Prosp., 32, 1–17.

Hill, N. R., and Levander, R., 1984, Resonances of low-velocity layers with lateral variations: Bull. Seis. Soc. Am., 74, 521–537.

Hron, F., and Mikhailenko, B. G., 1981, Numerical modeling of nongeometrical effects by the Alekseev-Mikhailenko method: Bull. Seis. Soc. Am., 71, 1011–1029.

Schneider, W. S., 1978, Integral formulation for migration in two and three dimensions: Geophysics, 43, 49–76.

Wu, R., and Aki, K., 1985, Scattering characteristics of elastic waves by elastic heterogeneity: Geophysics, 50, 582–595.